BIOCHEMISTRY
including biophysical chemistry & molecular biology
Article

Biochemistry **2009,** *48,* 11399–11411 11399
DOI: 10.1021/bi901371s

Kinetic Stability of the Flavin Semiquinone in Photolyase and Cryptochrome-DASH†

Michael J. Damiani, Gary N. Yalloway, Jessica Lu, Neahlanna R. McLeod, and Melanie A. O'Neill*

Department of Chemistry, Simon Fraser University, Burnaby, British Columbia, Canada V5A 1S6

Received August 6, 2009; Revised Manuscript Received November 3, 2009

ABSTRACT: Photolyases and cryptochromes (CRY) are structurally homologous flavoproteins with divergent functions. While photolyases repair UV-damaged DNA by photoinduced electron transfer from their FAD cofactor, CRY are involved in varied cellular processes, including light-dependent plant growth, regulation of mammalian circadian rhythm, and possibly magnetoreception. Despite their importance in Nature and human health, little is known about how they tune their FAD redox properties to achieve remarkable functional diversity. In this study, we reveal a kinetic mechanism, exploited by cyclobutane pyrimidine dimer photolyase (PL), for regulating the stability of its FAD semiquinone (sq). We find that the sq in CRY-DASH (*Synechocystis*) is substantially more reactive toward oxidation than in PL (*Anacystis nidulans*) and, using deuterium isotope and pH effects, show that rate-limiting proton transfer contributes to the exceptional kinetic stability of the PL sq. Through mutagenesis, we identify two PL-specific residues in the flavin binding pocket, Trp392 and Gly389 (Try398 and Asn395 in CRY-DASH, respectively), that ensure this kinetic stability, possibly through interactions with the adenine moiety of FAD and/or adjusting the polarity of the binding site. Significantly, these relatively distal residues have a much more profound impact than two amino acids closer to the FAD. By quantifying sq stability in a series of PL−CRY exchange mutants, our findings pave the way for investigations aimed at correlating sq stability with function in these proteins. As is being recognized with other flavoproteins, we expect that kinetic tuning of the rates of electron transfer will play a function-defining role in photolyases and cryptochromes.

Photolyases and cryptochromes (CRY)[1] are a functionally diverse family of light-responsive flavoproteins (*1*, *2*). Photolyases are enzymes that repair cyclobutane pyrimidine dimers (CPD) or 6-4 photoproducts in duplex DNA, by photoinduced electron transfer (ET) from their flavin adenine dinucleotide (FAD) cofactor; these reactions require base flipping (*3*−*6*). CRY do not recognize these substrates or catalyze these reactions (*7*, *8*), and their functions and mechanisms of action are ill-defined. Both plant and type I animal CRY (e.g., insects) are photoreceptors for synchronizing circadian rhythm (*9*, *10*), whereas type II animal CRY (e.g., humans) are light-independent regulators of the circadian clock, with potential roles in photoentrainment (*10*−*12*). Insect and avian CRY may also be photomagnetoreceptors for navigation (*13*). The functions of the CRY-DASH subclass (*14*−*18*) remain unclear, despite the fact that its members are very structurally homologous to CPD photolyases (PL), and both lack C-terminal extensions found in other CRY (*14*, *19*−*21*). The acronym highlights the close evolutionary relationship between CRY-DASH (found in, e.g., *Arabidopsis* and *Synechocystis*) and animal CRY (found in, e.g., *Homo* and *Drosophila*) (*14*, *18*). CRY-DASH can repair CPD in single-stranded regions of DNA (*8*, *21*), and compromised base flipping may account for its lack of physiological repair (*21*). However, the redox properties of PL and CRY-DASH are very different; CRY-DASH lacks the exceptional stability of the blue neutral semiquinone (sq) of *Escherichia coli* (*22*) and *Anacystis nidulans* (*23*) PL is absent in CRY-DASH *in vitro* (*14*−*18*). Protein-specific redox tuning is expected to be significant to the physiological functions of CRY-DASH and CRY generally (*24*).

The functional significance of sq stabilization by PL relates to its mechanism for DNA repair. Repair is initiated by a single ET from the fully reduced, anionic hydroquinone (hq), and the FAD cycles between sq and hq during catalysis (*1*, *25*). Thermodynamic stabilization of the hq is likely important. Recently reported values for the sq/hq potential (E_1) of approximately −50 to 16 mV, the same within error for *E. coli* and *A. nidulans* PL, are more positive than that of free flavin (E_1 = −101 mV) (*26*) and become larger by ∼65−75 mV when bound to substrate DNA (*27*, *28*). Sq stabilization is even more impressive. In both *E. coli* and *A. nidulans* PL, the sq resists oxidation by O_2 and strong chemical oxidants (*22*, *29*), as well as electrochemical potentials as high as 400 mV (*28*). Partial aerobic oxidation to the fully oxidized FAD (ox) occurs over days to months (*30*), depending on the temperature and solvent, while even excess potassium ferricyanide requires ∼3 days to achieve full oxidation (*31*). A stabilized sq that resists return ET with the geminate CPD radical anion may contribute to the near-unity quantum efficiency of PL (*32*). More generally, as in several other flavoproteins (*33*−*41*), sq stability may be used to adjust the degree of single and double ET (*38*). For single ET, a stabilized sq inhibits either complete oxidation, e.g., in flavodoxins (*33*−*35*)

†This work was supported by grants from the Michael Smith Foundation for Health Research (to M.A.O.).

*To whom correspondence should be addressed: Department of Chemistry, Simon Fraser University, Burnaby, British Columbia, Canada V5A 1S6. Telephone: (778) 782-5608. Fax: (778) 782-3765. E-mail: maoneill@sfu.ca.

[1]Abbreviations: CRY, cryptochromes; CPD, cyclobutane pyrimidine dimers; ET, electron transfer; FAD, flavin adenine dinucleotide; PL, CPD photolyase; sq, semiquinone; hq, hydroquinone; ox, oxidized; k_1, rate constant for hq oxidation; k_2, rate constant for sq oxidation; MTHF, methenyltetrahydrofolate; 8-HDF, 8-hydroxy-5-deazariboflavin; EDTA, ethylenediaminetetraacetic acid; PDB, Protein Data Bank.

Published on Web 11/04/2009

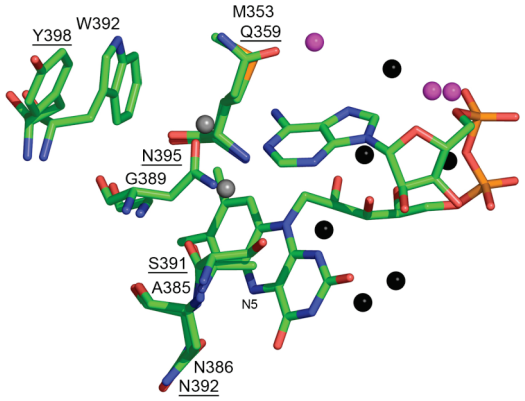

FIGURE 1: Overlay of crystal structures of *A. nidulans* PL (PDB entry 1qnf) (*44*) and *Synechocystis* sp. PCC6803 CRY-DASH (PDB entry 1np7, underlined residues) (*14*) highlighting distinct residues in the FAD binding pocket, the conserved N5-proximal Asn, and structurally conserved water molecules common to both proteins (black), unique to PL (gray), or unique to CRY-DASH (magenta).

and some reductases (*36*−*38*), or complete reduction, e.g., in *Bacillus megaterium* P450 BM3 reductase (*39*) or *Methylophilus methylotrophus* electron transfer flavoprotein (*40*, *41*), thereby preventing futile entry into dead-end redox states. Studies of each of these classes of flavoproteins have revealed a significant kinetic origin for sq stability derived from coupling of one of the two redox reactions to a proton transfer, along with associated changes in protein conformation to adjust the H-bonding pattern at the isoalloxazine N5(H) group (*33*−*41*). Just as the protein environment tunes the thermodynamic stability of its flavin redox states for function, so too does it control the rates of their ET reactions (*42*, *43*). Here, we show that the sq is kinetically stabilized in PL, through proton-coupled electron transfer, and we identify residues key to this stabilization, and its loss in CRY-DASH.

Ten of the residues closest to the FAD isoalloxazine are conserved between PL and CRY-DASH (*14*, *44*). This includes Asn386/392 (Figure 1), which likely uses its side-chain carbonyl to accept a H-bond from the N5(H) group of the neutral sq radical. In *E. coli* PL, substitution of this Asn for Ser abolishes sq stability *in vitro* together with catalytic activity *in vitro* and in cells (*32*). It is not known whether this Asn stabilizes the sq kinetically and/or thermodynamically. Moreover, in CRY-DASH, the similarly conserved Asn does not confer sq stability; other residues must define the impact of the N5-proximal Asn. We have targeted four conserved residues in the vicinity of the FAD cofactor in PL that are distinct in CRY-DASH (Figure 1). PL Ala385, which is also within H-bonding distance of the isoalloxazine N5 atom (∼4 Å), is replaced with Ser391 in CRY-DASH. PL Gly389 is ∼7−9 Å from the isoalloxazine N5 atom and adenine, while in CRY-DASH, the corresponding Asn395 is positioned to H-bond with N1 and the exocyclic amine of adenine. PL Met353 and Trp392 are even more distal from the isoalloxazine N5 atom (distances of ∼9 and 13 Å, respectively). Met353 has been proposed to mediate electron tunneling from FAD to DNA, and all proteins shown to catalyze CPD repair in duplex DNA have this Met; proteins lacking this activity have a different residue, e.g., Gln359 in CRY-DASH (*45*). PL Trp392, which stacks side on with bound CPD (*5*), is replaced with Tyr398 in CRY-DASH. Different orientations of these Tyr and Trp residues, with their rings flipped ∼180°, have been seen in CRY-DASH (*14*, *19*−*21*), and recently 6-4-PL (*6*, *24*), in unbound and bound forms.

In this study, we report large kinetic isotope and pH effects on the rate constants for FAD sq oxidation which reveal that proton transfer is rate-limiting in CRY-DASH, and especially PL. Two PL-specific resides, Trp392 and Gly389, independently ensure a high kinetic barrier to sq reactivity in PL. These residues have a much greater impact on sq reactivity than the more FAD-proximal Met353 or Ser395, and we propose models for their tuning of redox kinetics involving interactions with the adenine moiety of FAD and/or adjustment of the polarity of the binding site. These first insights into such a mechanism of redox regulation in PL and CRY are expected to advance recently proposed correlations between sq stability and function (*24*, *32*), unraveling of the biological roles of CRY, and understanding of flavoprotein redox tuning, generally.

MATERIALS AND METHODS

Protein Expression, Purification, and Characterization. Coding DNA for the PL and CRY-DASH mutants was generated by site-directed mutagenesis and sequences prior to protein preparation. *A. nidulans* photolyase and *Synechocystis* sp. PCC 6803 cryptochrome were prepared as previously described (*15*, *23*); analogous procedures were used for the mutants. Briefly, PL proteins (in pET3a vectors) were overexpressed in *E. coli* BL21(DE3)pLysS cells grown in 8 × 1 L batches at 37 °C. Protein expression was induced by addition of 600 μM IPTG at an OD_{600} of ∼0.9 (after ∼3−4 h), and cell growth was continued for 2 h at 37 °C. Cells were harvested by centrifugation (5000 rpm) at 4 °C for 10 min, and the resulting pellet was washed and resuspended in 3 × 20 mL of column buffer [10 mM KH_2PO_4/K_2HPO_4 and 100 mM NaCl (pH 7.0)], flash-frozen, and allowed to thaw overnight on ice. The cell-free extract was prepared by sonication followed by centrifugation (16000 rpm) for 1 h at 4 °C. The filtered cell-free extract was loaded onto a 5 mL heparin column, washed with 5 column volumes of column buffer to remove unbound protein impurities, and then washed with a salt gradient (from 100 to 900 mM NaCl in column buffer). All PL proteins eluted at salt concentrations of 450−650 mM NaCl, as monitored by sodium dodecyl sulfate−polyacrylamide gel electrophoresis (SDS−PAGE) and UV−vis spectroscopy. Elutions containing PL were pooled, exchanged into column buffer, reapplied to a heparin column, and eluted as described previously. The PL elutions were pooled and exchanged into DEAE-Sepharose column buffer [10 mM KH_2PO_4/K_2HPO_4, 40 mM NaCl, and 5 mM β-mercaptoethanol (pH 7.0)] and then applied to a DEAE-Sepharose column. PL was eluted with a salt gradient (from 80 to 200 mM NaCl) and assayed for purity by SDS−PAGE (Figure S1 of the Supporting Information). Pure fractions were combined, exchanged into storage buffer [10 mM KH_2PO_4/K_2HPO_4, 350 mM NaCl, and 10% glycerol (pH 7)], aliquoted, flash-frozen, and stored at −80 °C. The typical yield of pure PL and mutants was 2 mg/L.

GST-tagged CRY-DASH and its mutant (in pGEX vectors) were overexpressed in *E. coli* JM109 grown in 24 × 1 L batches at 37 °C. Protein expression was induced at an OD_{600} of ∼0.9 (after ∼3−4 h), by addition of 400 μM IPTG, and growth was continued overnight at 37 °C. Cells were harvested by centrifugation (5000 rpm) at 4 °C for 10 min, and the resulting pellet was washed and resuspended in 6 × 30 mL of column buffer [10 mM KH_2PO_4/K_2HPO_4, 140 mM NaCl, 5 mM DTT, and 5% glycerol (pH 7.4)], flash-frozen in liquid nitrogen, and allowed to thaw overnight on ice. The cell-free extract was prepared by sonication,

followed by centrifugation (16000 rpm) for 1 h at 4 °C, and filtration. The cell-free extract was applied to a 5 mL GST column and subsequently washed with 5 column volumes of column buffer, followed by elution using 10 mM glutathione in column buffer. The presence and purity of GST-CRY in the elutions were probed by UV−vis spectroscopy and SDS−PAGE. These consistently contain fusion protein (~83 kDa), together with a coeluting impurity (~60 kDa), as previously observed (Figure S2 of the Supporting Information) (*15*). The elutions were concentrated to a final volume of 2 mL (Centricon-10) and subjected to thrombin digestion (2 units/mg) at ambient temperature for 2−3 h. Complete cleavage of GST was confirmed by SDS−PAGE (Figure S2 of the Supporting Information). The resulting mixture was then applied to a 5 mL heparin column. Washing with 5 column volumes of column buffer elutes GST and the other protein impurity. A salt gradient (from 150 to 600 mM NaCl in column buffer) was then used to elute pure CRY-DASH. Elutions containing pure CRY-DASH (350−460 mM NaCl), as determined by UV−vis spectroscopy and SDS−PAGE (Figure S2 of the Supporting Information), were pooled, concentrated in storage buffer [10 mM KH_2PO_4/K_2HPO_4, 350 mM NaCl, and 10% glycerol (pH 7)], aliquoted, flash-frozen, and stored at −80 °C. The typical yield of pure CRY-DASH is 1 mg/L. Expression yields and the solubility of Y398W-CRY-DASH were significantly lower.

In these preparations, *A. nidulans* PL contains FAD only, since *E. coli* does not synthesize its antenna cofactor, 8-hydroxy-7-deazaflavin (8-HDF); *Synechocystis* CRY-DASH contains both FAD and its antenna cofactor, 5,10-methenyltetrahydrofolate (MTHF). The protein concentration and cofactor stoichiometry were determined as follows. (1) Absorption spectra of the fully oxidized holoproteins were taken to estimate the total protein concentration from A_{280}. The ε_{280} includes contributions from the protein (Trp and Tyr), oxidized FAD, and MTHF (CRY-DASH). For PL, A385S-PL, and M353Q-PL, full oxidation was achieved by incubating the protein at 4 °C with 10 mM potassium ferricyanide for a period of 3 days; excess ferricyanide was removed by exchange into storage buffer (Centricon-10). (2) The proteins were heat-denatured (100 °C for 5 min in storage buffer); precipitated protein was removed by centrifugation, and the absorption spectra of the released FAD were collected (this process destroys absorption by MTHF in CRY-DASH). This provides an accurate measure of the total concentration of FAD using its known ε value in solution. (3) The concentration of MTHF cofactor in CRY-DASH was estimated from its protein-bound absorption at 380 nm, after correction for absorption at that wavelength by FAD. The following extinction coefficients were used: for FAD, ε_{440} = 11300 M^{-1} cm^{-1} (*16*), ε_{380} = 10274 M^{-1} cm^{-1}, and ε_{280} = 21200 M^{-1} cm^{-1} (*46*); for MTHF, ε_{380} = 25900 M^{-1} cm^{-1} (*47*) and ε_{280} = 16000 M^{-1} cm^{-1} (*46*); for PL apoprotein, ε_{280} = 119860 M^{-1} cm^{-1} (18 Trp residues and 14 Tyr residues); for PLox, ε_{280} = 141060 M^{-1} cm^{-1}; for CRY-DASH apoprotein, ε_{280} = 120320 M^{-1} cm^{-1} (17 Trp residues and 18 Tyr residues); for CRYox, ε_{280} = 157520 M^{-1} cm^{-1}.

Oxidized PL, with a stoichiometric complement of its FAD cofactor, should have an absorbance ratio, A_{280}/A_{440}, of ~13. For both wild-type and mutant PL (Figure S3 of the Supporting Information), we consistently find A_{280}/A_{440} = 12−14, indicating near-quantitative preparation of the holoproteins. Oxidized CRY-DASH, if both the MTHF and FAD cofactors are stoichiometric, should have an A_{280}:A_{380}:A_{440} absorbance ratio of ~14:4:1. With wild-type CRY-DASH, we usually observe substoichiometric concentrations of each cofactor, typically 70−80% for both FAD and MTHF. Although we generated relatively little soluble Y398W-CRY-DASH to characterize extensively, it appears to contain a somewhat lower concentration of cofactors (50−60%) than the wild type (Figure S3 of the Supporting Information).

Sample Preparation. Proteins (20−30 μM) in 600 μL of PBS [12 mM KH_2PO_4/K_2HPO_4 and 350 mM NaCl (pH 7)] containing 10% glycerol and 10 mM EDTA (for photoreduction) were contained in a custom-built quartz anaerobic cuvette (1 cm path length) equipped with an indicator side arm filled with ~600 μL of 3 mM methyl viologen, 3 mM EDTA, and 40 μM FAD in PBS. The cuvette was made anaerobic by four cycles of evacuation/flushing with ultrapure argon; the cell was then sealed. The solution in the side arm was photoreduced (deep blue) with white light prior to each experiment. The indicator solution serves to soak up extraneous oxygen and provides a sensitive measure of its presence in the cell. Experiments at pH 5.4 were conducted in citrate buffer with 350 mM NaCl. We note that the citrate buffer at pH 7 causes a small decrease in sq reactivity relative to our phosphate buffer at the same pH. Samples for kinetic isotope experiments were prepared by repeated buffer exchange of oxidized proteins (*48*) into D_2O-PBS (four times with 15-fold excess deuterated buffer) and incubation at 4 °C in the dark overnight.

Oxidation Experiments and Kinetic Analysis. Absorption spectra were recorded at 10 ± 0.5 °C on a Varian Cary 100 spectrophotometer equipped with a temperature-controlled multicell holder. Spectra were scanned from 800 to 200 nm with a 1 nm step size, a 1 s integration time, and a 1 nm spectral bandwidth. Anaerobic protein samples, in the presence of EDTA as an electron donor, were photoreduced by irradiation with white light (300 W, ~10 cm) for 20−40 min in an ice−water bath, until they were fully reduced (*49*, *50*). Absorption spectra were recorded during the reduction to monitor the changes in FAD redox state (Figure S4 of the Supporting Information). Fully reduced, anaerobic samples were made aerobic by releasing the seal of the sample cell and allowed to react with O_2 at 10 °C for ~2−3 days. Time-dependent absorption spectra (~130) were recorded, using the Varian software scanning kinetics program, to monitor the decay of hq, the formation of ox, and the growth and decay of sq.

The changes in the concentration of each of the three species were analyzed according to the mechanism presented in Scheme 1, namely A to B to C kinetics, with a parallel A to C pathway. Assuming that each step is irreversible and proceeds with pseudo-first-order kinetics, the analytical expressions for the time-dependent concentrations of A (hq), B (sq), and C (ox) are given by eqs 1−3

$$[\mathrm{hq}]_t = [\mathrm{hq}]_o e^{-(k_1+k_3)t} \quad (1)$$

$$[\mathrm{sq}]_t = [\mathrm{hq}]_o \frac{k_1}{k_2-(k_1+k_3)}[e^{-(k_1+k_3)t} - e^{-k_2 t}] \quad (2)$$

$$[\mathrm{ox}]_t = [\mathrm{hq}]_o \left\{ \frac{k_1 k_2}{(k_1+k_3)[k_2-(k_1+k_3)]} + \frac{k_3}{k_1+k_3} \right\} [1 - e^{-(k_1+k_3)t}] - \frac{[\mathrm{hq}]_o k_1}{k_2-(k_1+k_3)}(1 - e^{-k_2 t}) \quad (3)$$

where $[\mathrm{hq}]_o$ is the initial concentration of hq. Multivariable analysis involving simultaneous fitting of the experimental data

Scheme 1: Oxidation Pathways for FAD hq and sq[a]

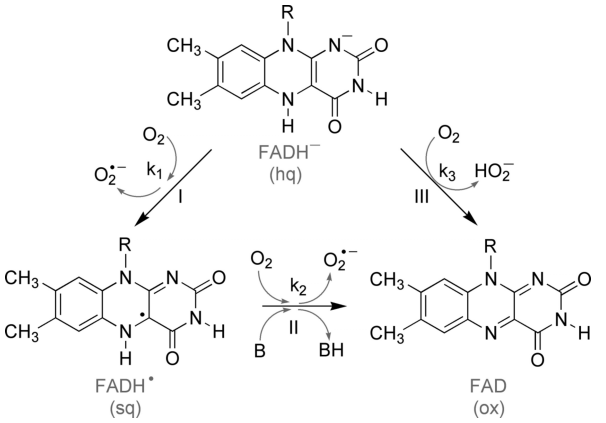

[a]R represents ribitol diphosphoadenosine.

at two wavelengths, 580 and 445 nm, to eqs 1−3 was performed (Microsoft Excel with Solver Program). These wavelengths were chosen since the sq is the only species to absorb at 580 nm, while ox absorbs strongly at 445 nm (at no wavelength is absorption of the hq dominant). The fitting algorithm evaluates the time-dependent concentrations, $[hq]_t$, $[sq]_t$, and $[ox]_t$, according to eqs 1−3, varying the three rate constants iteratively, to reach the best match with the experimental data. Specifically, the fit criterion was set to minimize the sum of the squared standard deviations between the model and the data at both 445 and 580 nm (χ^2). The χ^2 values for these simultaneous analyses typically fell in the range of $10^{-3}-10^{-4}$.

The calculated $[hq]_t$, $[sq]_t$, and $[ox]_t$ values are multiplied by their extinction coefficients at each wavelength for comparison with the input experimental data (absorbance vs time at 580 and 445 nm). We evaluated the extinction coefficients experimentally in our proteins (Figure S5 of the Supporting Information) by recording absorption spectra in the fully reduced, fully oxidized, or fully sq (PL only) state and then denaturing the protein to release the FAD and accurately measure its concentration (ε_{FAD} = 11300 M^{-1} cm^{-1} at 440 nm). Within experimental error ($\leq$10%), where measurable, these values do not vary significantly among the different proteins. Consequently, we have fixed the extinction coefficients to the following values in our kinetic analysis: at 580 nm, ε_{sq} = 5000 M^{-1} cm^{-1}; at 445 nm, ε_{ox} = 11500 M^{-1} cm^{-1}, ε_{sq} = 3670 M^{-1} cm^{-1}, and ε_{hq} = 1750 M^{-1} cm^{-1}. These values are within the range expected for flavins and flavoproteins. Small changes in ε values (e.g., 10−20%) generally do not notably change the shape of the kinetic profile or output rate constants. Significant changes in ε values generally prevent reasonable convergence between the model and data. The kinetic analysis according to eqs 1−3 also requires a value for $[hq]_o$. This may be evaluated from the absorbance of the fully reduced protein at the start of an oxidation experiment (ε_{hq} = 6000 M^{-1} cm^{-1} at 360 nm), from the absorbance of the sq at peak formation (when produced approximately quantitatively), and/or from denaturing the protein and releasing the FAD at the end of the experiment. These generally give consistent measures of total FAD concentration (within 1−2 μM for typical experiments with 20−30 μM total FAD). Experiments with Y392W-CRY were conducted at a lower concentration (1−2 μM) as we were unable to express reasonable yields of the soluble protein. Moreover, no sq was detected at this concentration. Consequently, quantitative kinetic analysis was not feasible.

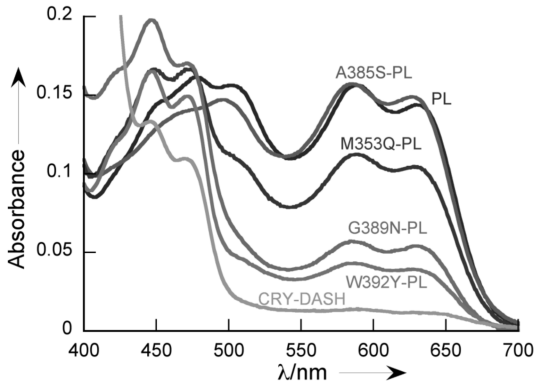

FIGURE 2: UV−vis absorption spectra of PL, PL mutants, and CRY-DASH in aqueous aerated buffer (pH 7) following complete purification. The concentration of each holoprotein was ~35 μM.

RESULTS

Targeted PL Mutants Exhibit a Range of sq Stabilities. Following overexpression in *E. coli*, isolation, and purification, all proteins contain near-stoichiometric amounts of noncovalently bound FAD [~100% except CRY-DASH (Figure S3 of the Supporting Information)]. The absorption spectra confirm a folate cofactor (MTHF) is also bound to CRY-DASH, as expected (*19*−*21*). Our PL preparations contain only FAD since *A. nidulans* PL uses 8-HDF as an antenna cofactor, and this is not synthesized by *E. coli*. Upon isolation of the PL proteins under aerobic conditions, the FAD hq, which presumably predominates in the cell (*1*, *25*), oxidizes only partially, and most of the FAD is in the sq form. This contrasts with free FAD where the hq is fully oxidized upon exposure to O_2 due to diffusion-controlled disproportionation of the sq, and rapid reaction of both hq and sq with O_2 (*42*). However, with exposure to air during complete purification (3 days), the PL proteins oxidize to different extents, as revealed by their colors. Colorless hq has a weak but defining UV band at 360 nm; blue sq is the only species absorbing between 500 and 700 nm, and yellow ox dominates absorption between 350 and 500 nm, with characteristic fine structure in protein-bound form (Figure S5 of the Supporting Information). Wild-type PL, A385S-PL, and M353Q-PL are blue after purification, while G389N-PL and W392Y-PL are yellow-green; significantly less sq is evident in their absorption spectra (Figure 2). CRY-DASH is yellow following isolation from the cell, and little sq is detected spectroscopically during or after purification.

Oxidation Reactions Reveal Kinetic Stabilization of the sq in PL That Is Modulated through Single-Site Mutation to Specific CRY-DASH Homologues. The rate constants and mechanisms for reaction of the FAD hq with molecular oxygen (Scheme 1) provide quantitative measures of the kinetic stability of the hq and sq toward oxidation (*34*, *38*). The initial step, both in solution and while protein-bound, is transfer of a single electron from the FAD hq to O_2, generating the caged sq/superoxide radical pair (*34*, *42*, *43*). The geminal superoxide may accept a second electron and a proton from the flavin N5 atom, either directly, or mediated through the formation of a C4(a)-(hydro)peroxide intermediate; following protonation of the resultant hydroperoxide anion, this pathway yields the two-electron transfer products, fully oxidized FAD and hydrogen peroxide (pathway III, Scheme 1). Such reactivity with molecular oxygen is characteristic of free flavin and flavoprotein oxidases (*42*). Alternatively, dissociation of the radical pair yields the neutral sq and superoxide (pathway I), as observed for

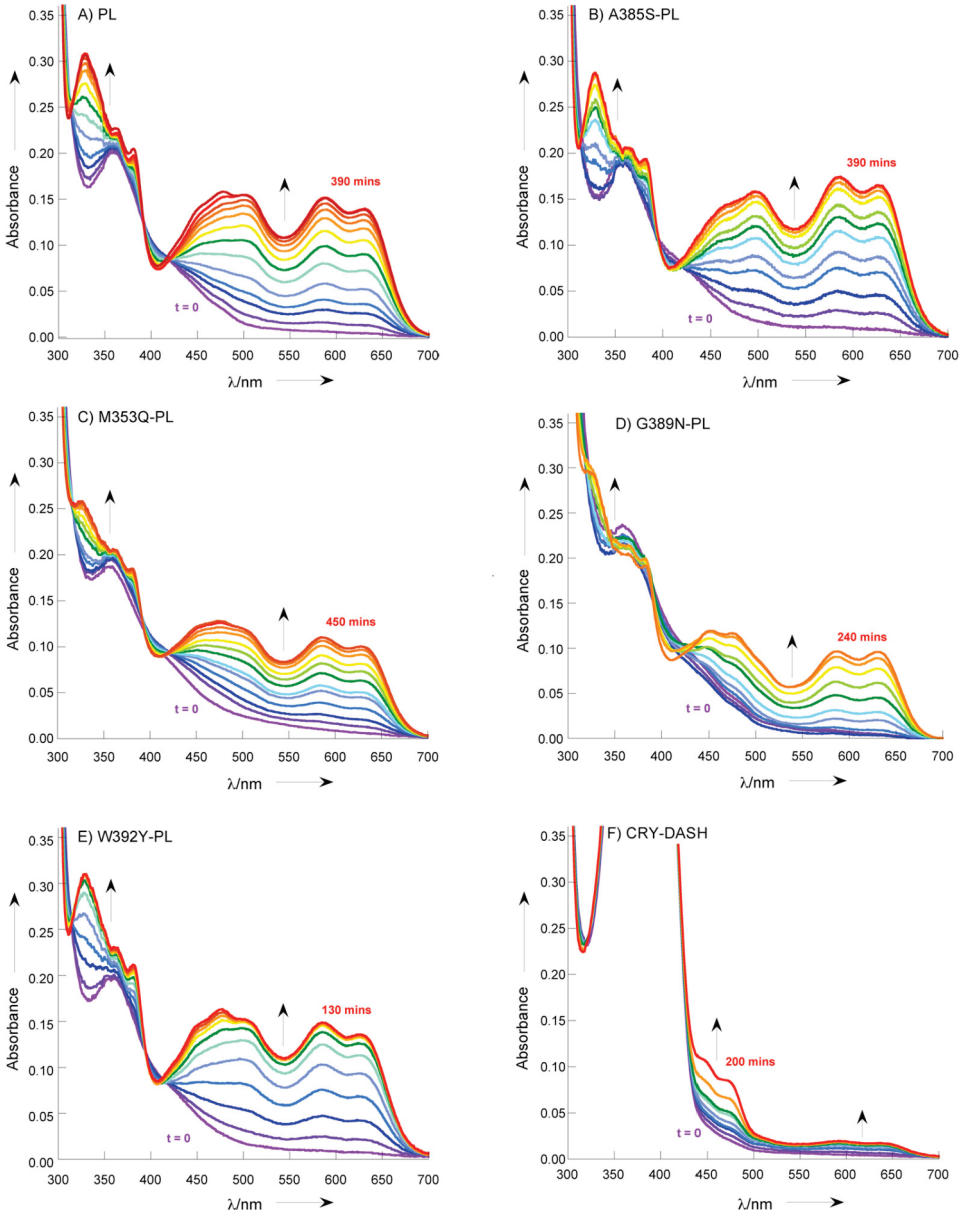

FIGURE 3: Oxidation of FAD hq in wild-type and mutant PL and CRY-DASH. Shown are time-dependent UV−vis absorption spectra for the first ~100−450 min following introduction of O_2 into fully reduced (A) PL, (B) A385S-PL, (C) M353Q-PL, (D) G389N-PL, (E) W392Y-PL, and (F) CRY-DASH. During this first phase of the oxidation reaction, the hq is consumed and accumulation of sq occurs. In PL and its mutants, hq oxidizes cleanly to the sq, while in CRY, significantly less sq builds up and concomitant ox formation is seen. Spectra are reported on the same scales. The strong absorbance between 320 and 420 nm in CRY-DASH is due to MTHF. Proteins were at a concentration of ~30 μM in phosphate buffer (pH 7).

electron transferases (*42*). The sq is itself susceptible to a second oxidation by single electron transfer to another molecule of O_2 (pathway II). Reaction of the sq requires both electron loss and deprotonation at N5 to complete the conversion to FAD ox.

The FAD hq, prepared by photochemical reduction of anaerobic samples of PL and CRY-DASH (Figure S4 of the Supporting Information), reacts with saturating concentrations of O_2 over a period of several hundred minutes. During this time, the hq is consumed and the sq grows in to reach a peak near quantitative formation in each of the PL proteins (Figure 3). This, together with several isosbestic points (420, 380, and 320 nm), suggests complete conversion of hq to sq through single ET to O_2, with production of transient superoxide (pathway I); direct two-electron oxidation of the hq (pathway III) does not appear to be competitive with sq formation in these proteins. The resultant sq is subsequently converted cleanly to fully oxidized FAD (Figure 4), and the expected isosbestic points (Figure S5 of the Supporting Information) are seen near 490 and 340 nm. Oxidation of the sq is also mediated by ET to O_2, but deprotonation of the isoalloxazine N5(H) atom is required to generate ox (pathway II), and the sq is much less reactive than the hq. Moreover, sq reactivity varies significantly among the PL proteins. A reaction time of ~2 or 3 days is required for complete conversion of sq to ox in W392Y-PL or G389N-PL, respectively. Importantly, spectra of anaerobic protein samples are unchanged over these times under similar conditions (Figure S6 of the Supporting Information), and FAD remains protein-bound throughout all experiments (Figure S3 of the Supporting Information). With wild-type PL, as well as its M353Q and A385S mutants, partial formation of ox is evident after 2 days, but most of the sq remains unreacted. In these proteins, some sq persists for weeks at 4 °C (Figure S7 of the Supporting Information). We note that the slow

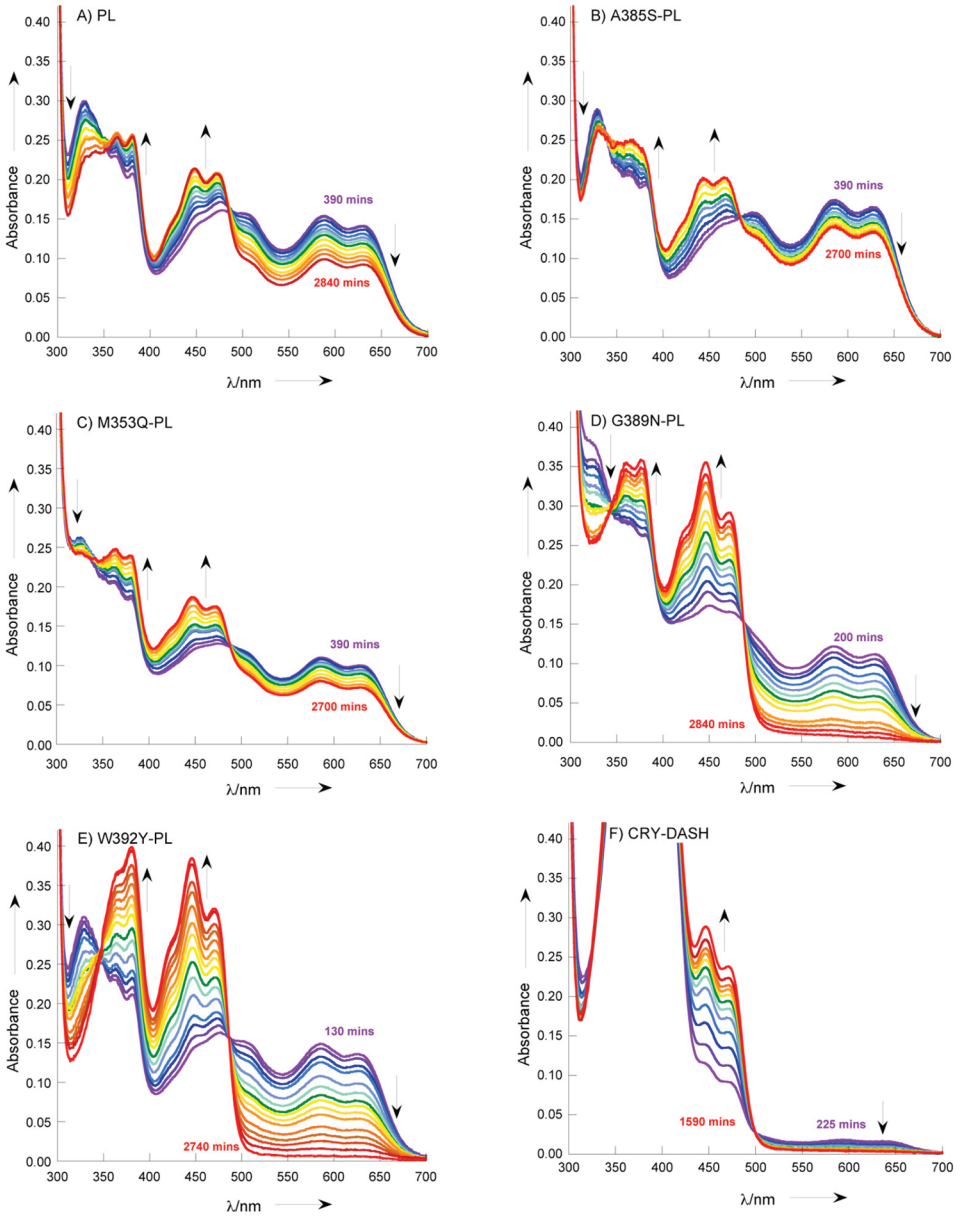

FIGURE 4: Different degrees of FAD sq oxidation in wild-type and mutant PL and CRY-DASH. Shown are time-dependent UV−vis absorption spectra profiling the reaction of O_2 with FAD sq in PL proteins (A−E as in Figure 3) and with FAD hq/sq in CRY-DASH (F). Each starting spectrum is at the time of peak sq formation (maximum absorption between 500 and 700 nm; for earlier time spectra of sq formation, see Figure 3). This closely matches the spectrum of pure sq in all PL proteins, and with time, the sq absorbance decreases and absorption bands characteristic of FAD ox grow in between 350 and 500 nm. A similar growth is seen in CRY-DASH; however, FAD ox dominates the spectra from the beginning. Spectra are reported on the same scales. The strong absorbance between 320 and 420 nm in CRY-DASH is due to MTHF. Proteins were at a concentration of ~30 μM in phosphate buffer (pH 7).

kinetics of sq decay and formation of fully oxidized FAD (ox) in wild-type PL and its M353Q and A385S mutants may contain some contribution from sq disproportionation.

The sq is the most reactive in CRY-DASH. This is clearly evident from the data presented in Figures 3 and 4. While the sq reaches its maximum detected concentration after reaction of the hq with O_2 for a similar time in all proteins ($t_{max} \sim 200-500$ min), only in CRY-DASH does the fully oxidized FAD form concomitantly, and the peak sq is no more than ~15% of the total FAD concentration. These results indicate that k_2 is significantly faster in CRY-DASH (i.e., $k_2 > k_1$) than in the PL proteins, and/or an alternative channel for direct two-electron oxidation (*17*) of the hq is competitive (pathway III, Scheme 1).

The oxidation kinetics were quantitatively analyzed according to the mechanisms outlined in Scheme 1, by simultaneous fitting of the experimental data at 580 and 445 nm to eqs 1−3 (Materials and Methods). The kinetic model closely reproduces the experimental data at both wavelengths (Figure 5). For the PL proteins, this analysis confirms that a simplified kinetic model is sufficient to describe the experimental data, due to the significant separation between the rate constants ($k_1 > k_2 \gg k_3$). In the multivariable analysis, the k_3 term consistently converges to zero, as direct two-electron oxidation is not competitive with sq formation. The predicted values of k_1 and k_2 closely match those from analysis of changes in sq concentration monitored at 580 nm alone, according to eq 2, where $k_1 + k_3 \sim k_1$. Moreover, since k_1 is at least ~10-fold larger than k_2 for all of the PL proteins, the pre-exponential term in eq 2 approaches unity, and analysis of the 580 nm kinetics with a simple first-order growth plus decay gives the same rate constants within experimental

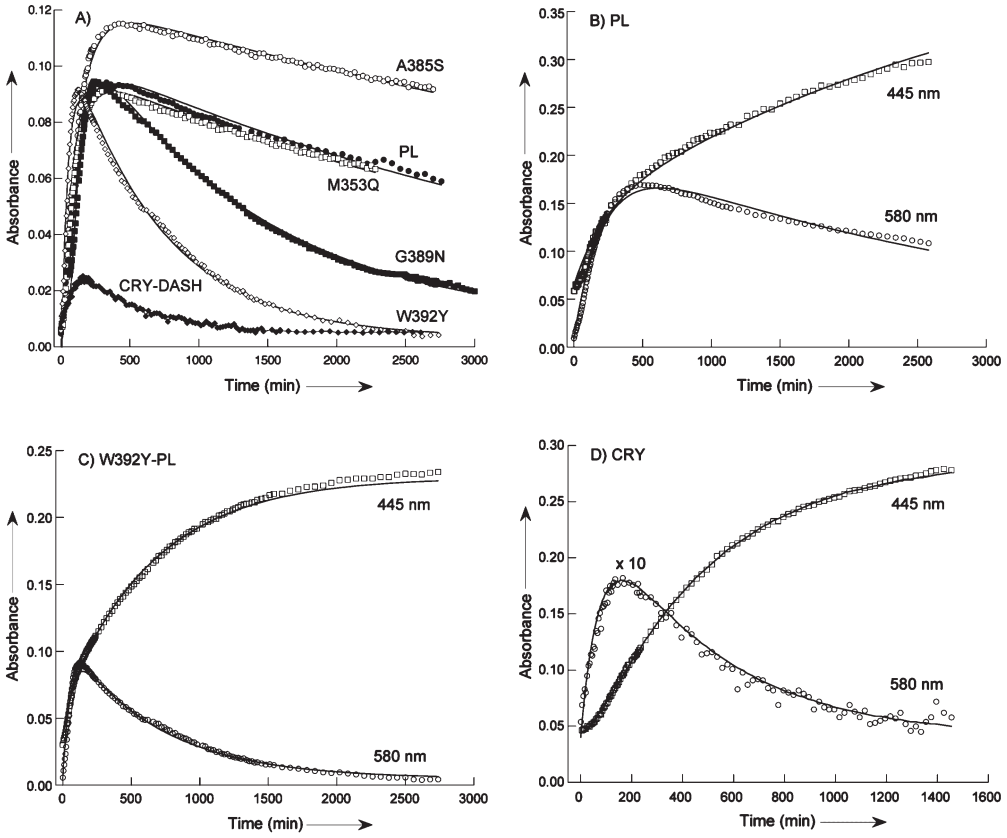

FIGURE 5: Distinct oxidation kinetics in wild-type and mutant PL, and CRY-DASH. (A) Growth and decay of the FAD sq monitored at 580 nm following introduction of O_2 into each anaerobic protein sample. For the PL proteins, lines are fits of the experimental data to eq 2 in the limit of $k_1 \gg k_3$ (i.e., A to B to C kinetics with no parallel A to C pathway). The absorbance values have been adjusted to account for small differences in concentration of each protein sample (20−30 μM), such that the yield of sq may be directly compared. (B−D) Comparison of the change in absorbance at 580 nm (sq absorbance only) and 445 nm (absorbance by all three species, with ox dominant) as a function of oxidation time in wild-type PL, where the sq is highly stabilized (B), W392Y-PL, where the sq is much more reactive (C), and in CRY-DASH, where $k_1 < k_2$ (D, 580 nm data multiplied by 10). The lines in each plot are the result of simultaneous fitting of the data (○ and □) to eqs 1−3; in no case does this analysis yield a non-zero k_3 term (χ^2 values of 7.7×10^{-3}, 3.1×10^{-3}, and 3.1×10^{-4} for PL, W392Y-PL, and CRY-DASH, respectively).

error (Table 1, Figure 5, and Figure S8 of the Supporting Information).

That multivariable analysis converges to the same rate constants as simpler models for the PL proteins is significant, as it lends confidence to the application of eqs 1−3 for modeling the oxidation kinetics in CRY-DASH. Here, given the low yield of sq, simultaneous fitting of the 580 and 445 nm data is required to establish the role of the two-electron pathway, and the relative magnitude of k_1 and k_2. Significantly, as in the PL proteins, pathway III is not required to model the kinetic data. The k_3 term also converges to zero in multivariable analysis of CRY-DASH oxidation, and the data at both wavelengths are described well by k_1 and k_2 alone (Figure 5 and Table 1). All attempts to force inclusion of a k_3 term were deleterious to the quality of the fit; a direct oxidation pathway does not match the observed lag, and slow buildup of ox. Instead, the low sq yield is ascribed to its slower formation, and especially its rapid reaction via pathway II. Multivariable analysis of the oxidation kinetics establishes that in CRY-DASH, unlike the PL proteins, $k_2 > k_1$ (Table 1).

The kinetic stability of the sq, k_1/k_2, varies as follows: A385S-PL > PL ~ M353Q-PL ≫ G389N-PL > W392Y-PL ≫ CRY-DASH (Table 1). For the PL proteins, hq oxidation is at least 10−100-fold faster than sq oxidation. This reactivity ratio may be even higher for the very persistent sq in PL, A385S-PL, and M353Q-PL. Continuous monitoring of the very slow sq oxidation in these proteins is not feasible. The sq concentration measured after long reaction times (up to 30 days) suggests that the rate constants for sq oxidation may be considerably smaller than those estimated from fitting ≤25% of their decay recorded over 2 days (Figure S7 of the Supporting Information). The k_2 values presented in Table 1 for PL, A385S-PL, and M353Q-PL are upper limits. The significant variation in the k_1/k_2 ratio in the PL proteins is dominated almost exclusively by differences in sq oxidation, since the rate constant for hq oxidation is similar in all proteins [W392Y-PL is slightly faster within experimental error (Table 1)]. While substitution of Met353 for Gln has little impact on sq stability, replacing Ala385 with Ser further enhances the sq stability of wild-type PL. In contrast, the kinetic stability of the sq is significantly reduced in W392Y-PL and G389N-PL, since their k_2 values are at least 10-fold faster than that of the wild type. The sq oxidation rates in these two proteins, especially W392Y-PL, more closely resemble that in CRY-DASH than that in wild-type PL; however, the overall kinetic stability of the sq in CRY-DASH is further diminished by a larger kinetic barrier to sq formation. In CRY-DASH, sq formation is slower than its decay.

sq Oxidation is Rate-Limited by Proton Transfer in PL and CRY-DASH. The lack of competitive two-electron oxidation of the hq in the PL proteins and CRY-DASH may not be surprising, given that complete oxidation also requires proton transfer, while conversion of hq to sq does not. The significance of proton transfer to sq kinetic stability in the PL proteins was revealed by the large deuterium isotope effect for its oxidation.

Table 1: Oxidation Kinetics of FAD hq and sq in Wild-Type and Mutant PL and CRY-DASH[a]

protein	k_1 ($\times 10^{-5}$ s^{-1})[b]	k_2 ($\times 10^{-5}$ s^{-1})[b]	k_1/k_2
PL	12 ± 2	< 0.4[c]	> 30
A385S-PL	13 ± 2	< 0.2[c]	> 65
M353Q-PL	14 ± 4	< 0.4[c]	> 30
G389N-PL	20 ± 3	1.2 ± 0.1	17
W392Y-PL	27 ± 4	2.6 ± 0.4	9
W392Y-PL (pH 5.4)[d]	27 ± 5	< 0.5[c]	> 68
PL (D_2O)	11 ± 2	< 0.1	> 110
W392Y-PL (D_2O)[d]	13 ± 5	< 0.6	> 20
CRY-DASH	4 ± 1	19 ± 2	0.2

[a]Averages and standard errors of three or four experiments. [b]For PL and PL mutants, the rate constants are derived from fitting the sq absorbance (580 nm) vs time to a first-order growth (k_1) plus decay (k_2). This analysis yields the same values, within experimental error, as fitting the 580 nm data to an A to B to C kinetic scheme, or simultaneous fitting of the 580 and 445 nm data to this scheme with inclusion of a parallel A to C pathway (eqs 1−3). For CRY-DASH, the rate constants are those obtained from simultaneous fitting of the 580 and 445 nm data to eqs 1−3. [c]Upper limit from fitting partial decay: 0.40 ± 0.04 for PL, 0.18 ± 0.02 for A385S-PL, 0.38 ± 0.04 for M353Q-PL, and 0.48 ± 0.08 for W392Y-PL. [d]Average of two replicates.

In aqueous buffer at neutral pH, decay of the sq in W392Y-PL is complete within 2700 min (Figure 6). Replacement of the exchangeable protons, including the N5(H) group of FAD, with deuterium (*48*) decreases the rate constant for sq oxidation by ~4-fold [k_2 (Table 1)], and more than ~60% of the sq persists after the same reaction time (Figure 6). The same experiment with the very unreactive sq in wild-type PL likewise decreases its rate constant for oxidation by a factor of ~4 (Figure 6 and Table 1). In both proteins, the rate constant for hq to sq conversion (k_1) is not significantly affected by deuterium exchange. These large kinetic isotope effects, near the maximum for N−H bond cleavage, given secondary solvent isotope effects, indicate that sq−ox interconversion involves proton-coupled ET. Results at lower pH are consistent with this conclusion. In a more acidic environment, the sq lifetime increases by ~5-fold (Figure 6 and Table 1). With CRY-DASH, deuterium exchange or reduction in pH nearly doubles the low yield of sq (Figure S9 of the Supporting Information). The ~2-fold increase in sq lifetime indicates that proton transfer is also rate-limiting with respect to sq oxidation in CRY-DASH, although to a lesser extent than in the PL proteins.

sq Kinetic Reactivity Impedes Equilibrium Measurements of Redox Potentials. Rate-limiting proton transfer in sq−ox interconversion also plays a role in electrochemical measurements of the redox potentials of these proteins. Investigations of *E. coli* and *A. nidulans* PL found that E_2 could not be measured, either due to instability of ox (*27*) or due to a lack of sq oxidation at potentials of up to 400 mV (*28*). However, with sufficient time, PL from both organisms may be oxidized at lower potentials, and the oxidized proteins are stable (Figure S3 of the Supporting Information) (*30*, *31*). We suspect that evaluation of E_2 may be limited not so much by its high positive value as by a kinetic barrier that prevents complete oxidation (*36*, *37*, *40*, *41*). In standard redox titrations with wild-type *A. nidulans* PL, we measure the same E_1 value as previously reported (*28*). However, we also observe partial oxidation of the sq, given extended equilibration times [5−10 h (Figure S10 of the Supporting Information)], analogous to partial reduction observed in redox titrations of electron transfer flavoprotein (*41*). As in this

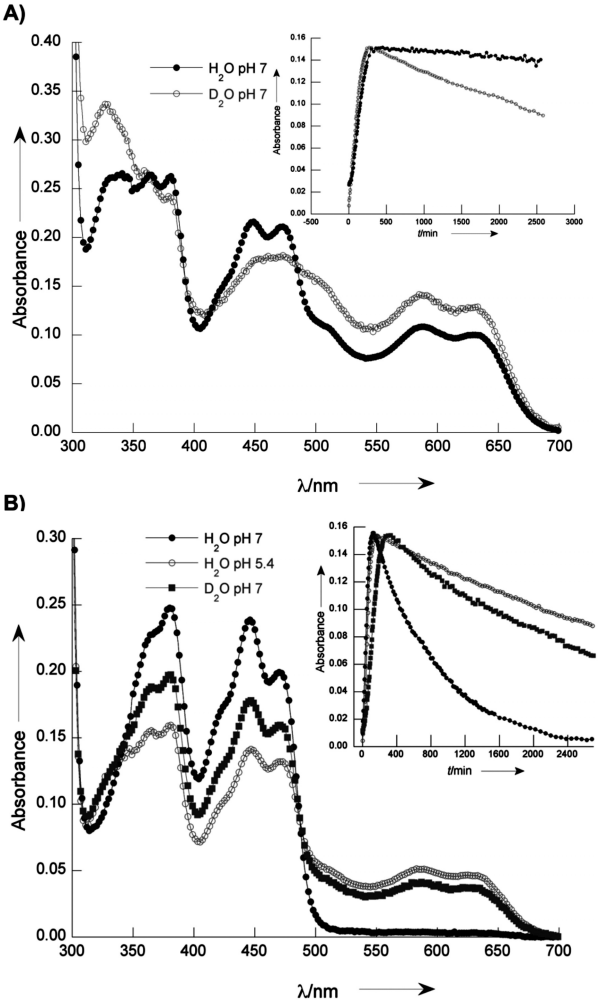

FIGURE 6: Evidence that oxidation of PL-bound sq proceeds by proton-coupled ET. Shown are the spectra ~2700 min after exposure of fully reduced PL (A) or W392Y-PL (B) to O_2 in acidic solution (H_2O pH 5.4), a neutral solution (H_2O pH 7), or at pH 7 following replacement of exchangeable protons with deuterium (D_2O, pH 7). In a neutral aqueous solution, W392Y-PL is completely oxidized during this time, while in H_2O at pH 5.4 or D_2O at pH 7, considerable absorbance by the sq at wavelengths of ≥500 nm remains. Similarly, the oxidation kinetics of the slowly decaying sq in wild-type PL are further reduced by deuterium exchange. The kinetics at 580 nm (insets) highlight the significant decrease in sq reactivity at lower pH, or following deuterium exchange. The protein concentration was ~25 μM.

experiment and others (*36*, *37*, *40*, *41*), equilibration becomes increasingly slow, inhibiting measurements of potentials. Furthermore, in contrast to oxidative titrations with both PL and W392Y-PL, where sq is clearly observed, sq is not detected in reductive titrations beginning with either fully oxidized protein (Figures S11 and S12 of the Supporting Information).

That the sq monitored during oxidative titrations may be a kinetic product is also suggested by the very slow disproportionation (> 160 h) of the PL sq under anaerobic conditions (Figure S13 of the Supporting Information). While disproportionation is greatly accelerated in W392Y-PL (~20 h), both proteins equilibrate too slowly for stepwise spectroelectrochemical titrations to evaluate their redox potentials. For CRY-DASH, it is instead the kinetic instability of its sq that limits its accumulation (we find no more than ~15% in redox titrations), and measurement of E_1 and E_2. Thus, while the redox potentials of the FAD cofactor likely also differ among these proteins, the intrinsic kinetic reactivity of their sq presents a major obstacle to thermodynamic

characterization. The importance of regulating redox kinetics in other flavoproteins is increasingly being recognized (*34*−*37*, *40*, *41*), and here we have focused on identifying residues that regulate the rates of proton-coupled ET in PL and CRY-DASH. We suspect that the kinetic stability of the sq may play a function-defining role in PL and CRY.

DISCUSSION

CRY and PL use a common flavin adenine dinucleotide (FAD) cofactor and homologous protein scaffold to accomplish numerous, seemingly dissimilar functions. PL are light-driven, DNA repair enzymes, found in a variety of bacteria and eukaryotes, although absent in most mammals (*1*). CRY are widely distributed in all kingdoms of life and involved in numerous fundamental biological processes (*1*, *2*, *8*−*14*). Like PL, many of their activities require light. For instance, plant and type I animal CRY (e.g., insects) are photoreceptors for synchronizing circadian rhythm, for regulating plant growth and development (*9*, *10*), and possibly for insect and avian geomagnetic navigation (*13*). A light-responsive role for type 2 animal CRY (e.g., humans) has yet to be found; however, these proteins also participate in the circadian clock as light-independent transcriptional repressors (*11*, *12*). Also like PL, photoinduced (or ground state) ET mediated by FAD may play a role in the many functions of CRY (*17*). Differences in redox properties among various CRY and PL have become apparent over the past few years (*28*, *51*−*54*), and a recent study proposes that regulation of sq stability is generally essential, with local tuning of the FAD environment acting to achieve functional diversity (*24*). While this is clearly a critical correlation to establish, little is known regarding the regulation of redox properties in either CRY or PL.

We have focused on comparative studies of PL and the CRY-DASH subclass to begin understanding redox tuning in this family of proteins. CRY-DASH is structurally very homologous to PL (*5*, *14*, *19*−*21*, *44*), both in global protein architecture (including its lack of a species-specific C-terminal extension) and in conservation of FAD-binding residues. It also shares some functional remnants of PL. While all CRY have lost the ability to function as PL in the cell, CRY-DASH does catalyze repair of CPD within single-stranded regions of DNA (*8*, *21*). These features, coupled with the fact that it is found in all kingdoms of life and is evolutionarily close to animal CRY (*14*, *18*), suggest that studies of CRY-DASH may be key to revealing molecular origins of evolution in PL and CRY. Our results establish that sq oxidation in PL and CRY-DASH is rate-limited by proton transfer. Through mutagenesis, we identify two residues, relatively distal from the FAD, that are essential to sq kinetic stability in PL, and gain first insights into the origin of enhanced sq reactivity in CRY-DASH. The conservation pattern of these residues throughout the PL and CRY family indicates that they are functional keystones. In the discussion to follow, we first consider alternative explanations for the distinct sq reactivity in PL, its mutants, and CRY-DASH and then propose two mechanisms by which the residues at positions 389 and 392 (PL numbering) may tune the rate constants for PCET.

Intraprotein versus Solution Oxidation Mechanisms. The variation in oxidation rate constants observed here among PL, its site-specific mutant, and CRY-DASH is not unexpected. Flavoproteins can dramatically tune the kinetics of their reactions with molecular oxygen, at least over a range of 10^6 (*42*, *43*). These reactions are ascribed to direct collision of O_2 with the protein-bound flavin hq or sq. Flavin accessibility is not thought to play a significant role in kinetic tuning since O_2 can readily enter flavin binding sites either directly or by diffusing through the fluctuating protein matrix (*43*). In contrast, in many flavoproteins, including PL and CRY, dissociation of the flavin tends to be quite restricted thermodynamically and kinetically, and the cofactor is often tightly buried within the protein. Consequently, flavin oxidation mechanisms involving dissociation of a non-covalent cofactor, reaction with O_2 in solution, followed by rebinding, are generally not considered. Such a rationale may be offered in support of an intraprotein oxidation mechanism for the proteins investigated here. Dissociation of FAD from these proteins is very difficult because the cofactor is integral to the protein fold and stability. The conditions required for apoprotein generation, e.g., dialysis for >30 days at pH ~4 and against 100 mM KCl for *A. nidulans* PL (*29*), attest to the very tight binding of the cofactor. Thus, k_{off} is expected to be very slow, and not competitive with oxidation in the active site. This expectation is borne out by high-resolution structural data that reveal a flavin unable to exit without (partial) protein unfolding; however, an access channel to the FAD large enough for O_2 and water to easily penetrate exists. It is further corroborated by recent measurements of k_{off} of $\sim 8 \times 10^{-5}$ and $\leq 3 \times 10^{-5}$ s^{-1} for dissociation of FAD ox ($K_D \sim 1$ μM) and hq ($K_D \sim 8$ nM), respectively, from *E. coli* PL (*55*). We expect that the sq dissociation rate constant may be even slower.

We can more directly address the possibility of a dissociation−oxidation−rebinding mechanism with our current experimental data. If such a mechanism were operative, dissociation (or possibly rebinding) would be rate-limiting, since oxidation in solution occurs with a rate constant of 10^4 M^{-1} s^{-1} (*42*). The oxidation kinetics we report would thus correspond to these binding kinetics. In this case, one would expect at most a small (no more than ~8%) binding isotope effect on the kinetics (*56*). Instead, we observe large kinetic isotope effects for sq oxidation, on the order of ~4-fold for both the wild type and W392Y-PL. These are consistent with N−H(D) bond cleavage in the rate-determining step, and oxidation within the protein as the dominant mechanism. Intraprotein oxidation is also not surprising given the anticipated redox potential of the FAD sq/ox couple (E_2) within wild-type PL. This potential may be predicted using thermodynamic cycles that relate differences in binding affinity of each of the redox states to differences in their free and protein-bound redox potentials (eq 4),

$$\Delta G_{hq} - \Delta G_{ox} = \Delta\Delta G = -F(E_2 - E_2^{free} + E_1 - E_1^{FREE}) \quad (4)$$

where F is Faraday's constant (*57*). Using the known potentials of the two redox couples for free FAD, −101 and −313 mV for E_1 and E_2, respectively (*26*), and the recently reported E_1 value for wild-type PL of −50 mV (*28*) yields the following expression for E_2:

$$E_2 \text{ (volts)} = \frac{\Delta\Delta G + 8.39 \text{ kcal mol}^{-1}}{-23.06 \text{ kcal mol}^{-1} \text{ V}^{-1}} \quad (5)$$

At ambient temperature (293 K), $\Delta\Delta G$ may be evaluated according to eq 6

$$\Delta\Delta G = -0.58 \times \ln\left(\frac{K_{hq}}{K_{ox}}\right) \quad (6)$$

where K_{hq} and K_{sq} represent the hq and sq association constants, respectively. For PL, the hq binding affinity is expected to be

significantly higher than that of ox (*58*). Recent measurements reporting dissociation constants of ~8 nM and ~1 μM for hq and ox of *E. coli* PL, respectively (*55*), indicate that binding of hq is at least 125-fold stronger. Using these relative binding affinities, eqs 5 and 6 predict $E_2 \sim -242$ mV in wild-type PL. If $K_{hq} \sim 1000K_{ox}$, then $E_2 \sim -190$ mV. Even if K_{hq} is as much as $10000K_{ox}$, the predicted E_2 of approximately −130 mV is still quite small. With these potentials, oxidation of the sq by O_2 [$E = -150$ mV (*59*)] is thermodynamically favored and/or feasible in the protein active site.

Structural Influences. As is the case with any mutagenesis study that aims to investigate protein structure−function relationships, it is possible that a mutation may impact protein fold. For instance, destabilization of the native PL fold in favor of an alternative structure that alters the FAD binding pocket could contribute to the reduced sq stability in W392Y-PL or G389N-PL. The evidence against this as the dominant effect is first the fact that the absorption spectra of FAD bound to each of the four mutants are identical to that of wild-type PL. Relatively subtle differences in binding site microenvironment and polarity may be expected to shift the position of the FAD absorption bands (*29*). Second, the mutant proteins exhibit stability in solution that is comparable to that of wild-type PL, as gauged by overexpression yields, solubility, and especially the maintenance of structural integrity and cofactor binding through multiple cycles of oxidation and reduction lasting at least several days. If the mutations are changing the protein fold, the non-native structures provide comparable FAD binding interactions and overall stability.

A difference between the CRY-DASH and PL proteins investigated here is the presence or absence, respectively, of an MTHF cofactor. Although the second cofactor is not functionally essential and is >15 Å from the FAD in PL and CRY-DASH, one may question whether the presence of MTHF destabilizes the sq in CRY-DASH. However, CRY-DASH lacking an MTHF cofactor does not exhibit enhanced sq stability. The E149A mutant *A. thaliana* CRY-DASH does not bind MTHF (*19*). Absorption spectra of this protein following purification under aerobic conditions indicate that it contains its FAD cofactor in nearly fully oxidized form. In addition, the photoreduction kinetics of CRY-DASH with and without its MTHF antenna are identical, and both proceed with no accumulation of sq (*19*). Similarly, the presence of the MTHF cofactor does not cause loss of sq stability in PL. A large body of literature attests to the stability of the sq in *E. coli* PL (which contains MTHF) and suggests that, when subject to the same conditions, sq stability is comparable in *E. coli* and *A. nidulans* PL. Furthermore, the redox potential of their hq/sq couple is the same within experimental error (*28*), and both sq display a kinetic barrier to oxidation; no oxidation is observed upon application of potentials as high as 400 mV (*28*), or addition of a 10-fold of excess potassium ferricyanide (*22*). Together, these observations suggest that the MTHF cofactor has relatively little impact on the sq stability and FAD redox properties in PL and CRY-DASH.

Mechanisms for Tuning Kinetics of Proton-Coupled Electron Transfer in PL and CRY-DASH. The proton acceptor or donor in FAD redox cycling in PL and CRY-DASH has not yet been identified, and there is no obvious base or acid in the vicinity of the FAD (*14*, *44*). The N5-proximal Asn [PL, Asn386 (Figure 1)] is replaced with Asp or Cys in plant CRY (e.g., *A. thaliana* CRY1) or type I animal CRY (e.g., *Drosophila melanogaster*), respectively. Since the sq in the former exists as a protonated, neutral radical, while it is an unprotonated radical anion in the latter, the Asp was initially proposed to directly participate in proton transfer during sq−ox interconversion in plant CRY (*51*). However, in the Cys-Asp mutant *D. melanogaster* CRY, the sq remains unprotonated, and proton transfer was proposed to be conducted by a bound water molecule(s) (*54*). Interestingly, the Cys-Asn mutant yielded a protonated, neutral sq that was quite stable toward reaction with O_2 (*54*). Thus, while the N5-proximal residue may not act in proton transfer, an Asn at this position clearly stabilizes the neutral sq in type 1 animal CRY as well as PL, perhaps through formation of a hydrogen bond with the protonated N5(H) group using its side-chain carbonyl (*32*). This key residue is likewise found in type 2 animal CRY (e.g., human CRY1 and CRY2), and attenuated transcriptional repression by Asn-Cys/Asp mutants suggests a functional role for this Asn in mammalian circadian rhythm (*24*). As type 1 animal CRY have a Cys at this position, a stable neutral radical may not be required for their function. Similarly, kinetic destabilization of the sq in CRY-DASH is likely significant with respect to its functional divergence from PL, but it has evolved through mutation at other sites, while conserving the N5-proximal Asn. An analogous strategy may be exploited by 6-4-PL, since this Asn is also conserved, but the sq stability of PL is not. Purified samples of 6-4-PL contain mostly oxidized FAD, and the sq radical generated by photoreduction has been reported to fully reoxidize within minutes of exposure to O_2 (*48*, *60*).

While sq formation is ~3-fold slower in CRY-DASH than in *A. nidulans* PL, sq oxidation, which requires rate-limiting deprotonation, is >20 times faster in CRY-DASH (Table 1). sq oxidation may be accelerated with an increase in the rate of electron or proton transfer, as well as conformational rearrangement that swaps H-bond acceptor for donor, upon deprotonation at the FAD N5(H) group. The rate of ET is governed, in part, by electron density distribution in the sq, which in PL is localized mainly on the central and pyrimidine rings of the isoalloxazine (*61*). However, the unusual U-shaped conformation of the FAD cofactor in these proteins affords intramolecular stacking and possible delocalization onto adenine. In structures of CRY-DASH, the side chain of Asn395 forms a hydrogen bond with N1 and the exocyclic amine of adenine (*14*, *19*−*21*). Interestingly, this Asn is conserved in 6-4-PL, and the same hydrogen bonding pattern with adenine was recently reported (*6*, *24*). With Gly389 at this position, these interactions are not possible in PL; instead, two conserved water molecules apparently fill the gap (Figure 1). The Asn−adenine interaction may contribute to enhanced kinetic reactivity of the sq in CRY-DASH, G389N-PL, and 6-4-PL (*48*, *60*) by, for example, decreasing the degree of electron delocalization onto adenine. Type 1 animal CRY also have an Asn at this position, while in plant CRY, it is a Gly-like PL. The identity of this residue may play a function-defining role by regulating FAD redox properties mediated through its adenine moiety.

The polarity of the FAD binding site is also higher in CRY-DASH, due to more bound waters, and replacement of PL Trp392, Gly389, Ala385, and Met353 with residues of higher polarity (Figure 1) (*14*, *19*−*21*). This may accelerate water-mediated proton transfer and contribute to the increased rate constants for sq oxidation in G389N-PL, as well as in W392Y-PL. The Trp is highly conserved in most PL and animal CRY, while it is a Tyr in CRY-DASH and plant CRY. In PL, this Trp stacks with the CPD (*5*) and is functionally essential. The ~100-fold loss of catalytic activity of the W392F mutant has been attributed to weakened substrate binding (*62*). However, in

6-4-PL, the corresponding Trp-Ala mutant exhibited substrate binding comparable to that of the wild type, but significantly diminished catalytic activity (*63*). In addition, *Saccharomyces cerevisae* PL, which is unusual in having a Phe at this position, is the only PL known to resist oxidation to the sq when isolated from cells (*64*). Although it is relatively distal from the FAD, we predict that this residue may also be a functional keystone in PL and CRY, through its impact of FAD redox properties. The data presented here show that replacement of Trp in PL with the more polar Tyr increases sq reactivity such that it approaches that of CRY-DASH. The residue at this position has a greater impact on sq reactivity than more FAD-proximal PL Met353 and Ala385, where mutation to CRY-DASH homologues had little, or an opposite effect, on reactivity. In the context of CRY-DASH, mutation of Tyr398 to Trp does not enhance sq stability. If anything, this mutation increases sq reactivity, by further reducing the k_1/k_2 ratio, or shifting the balance to direct two-electron oxidation of the hq (Scheme 1), since no sq is detected during oxidation of Y398W-CRY (Figure S14 of the Supporting Information). As with the N5-proximal Asn in PL and CRY, and as seen in other flavoproteins (*41*), the impact of conserved residues on redox reactivity may differ within homologous proteins, especially when proton transfer and/or conformational motion also contributes to the rates of ET. While subtle, local structural changes at keystone residues may regulate FAD redox or protonation state and function in PL and CRY (*24*), these changes must involve correlated interactions at multiple sites and/or with bound water.

Functional Significance of sq Stability in PL and CRY. In *E. coli* PL, mutation of strictly conserved Asn386 has been shown to destabilize the sq and also deactivate CPD repair (*32*). However, at least in the context of single-stranded substrates, CRY-DASH is as active as PL (*8*, *21*), despite its highly destabilized sq. The functional requirement of PL for a stabilized sq may be more definitively explored with the mutants characterized here, which destabilize or stabilize the sq; M353Q-PL may provide an interesting test, since Met353 has been proposed to be function-defining in PL (*43*), yet its mutation does not alter sq stability. Like the evolutionary split in redox regulation in P450 reductases (*36*), the impressive functional diversity of CRY may be rooted in the control of FAD redox properties, especially sq stability (*24*). Understanding how diverse sq reactivity is achieved, and how it correlates to function, is central to resolving the biological roles of CRY.

ACKNOWLEDGMENT

We are grateful to Takeshi Todo and Akira Yasui for providing the genes encoding *Synechocystis* sp. 6803 cryptochrome (CRY-DASH) and *A. nidulans* PL, respectively. We thank Paul Percival and Jean-Claude Brodovitch for their assistance with kinetic analysis.

SUPPORTING INFORMATION AVAILABLE

SDS−PAGE analysis of CRY-DASH, PL, and PL mutants (Figures S1 and S2); UV−vis absorption spectra for evaluating cofactor stoichiometry (Figure S3), monitoring protein photoreduction (Figure S4), presenting the extinction coefficients of the three FAD redox states in PL (Figure S5), monitoring the stability of anaerobic reduced proteins (Figure S6), and following long-term oxidation of PL (Figure S7); comparative analysis of oxidation reactions in A385S-PL and W392Y-PL with A to B to C kinetics versus a double first-order exponential expression (Figure S8); spectroscopic and kinetic evidence for proton-coupled electron transfer in CRY-DASH (Figure S9); spectroelectrochemical data for PL and W392Y-PL (Figures S10−12); UV−vis absorption spectra monitoring disproportionation of PL and W392Y-PL (Figure S13); and UV−vis absorption spectra monitoring oxidation of Y398W-CRY-DASH (Figure S14). This material is available free of charge via the Internet at http://pubs.acs.org.

REFERENCES

1. Sancar, A. (2003) Structure and function of DNA photolyase and cryptochrome blue-light photoreceptors. *Chem. Rev. 103*, 2203–2237.
2. Lin, C., and Todo, T. (2005) The cryptochromes. *Genome Biol. 6*, 220–229.
3. Vande Berg, B. J., and Sancar, G. B. (1998) Evidence for Dinucleotide Flipping by DNA Photolyase. *J. Biol. Chem. 273*, 20276–20284.
4. Christine, K. S., MacFarlane, A. W.IV, Yang, K., and Stanley, R. J. (2002) Cyclobutylpyrimidine Dimer Base Flipping by DNA Photolyase. *J. Biol. Chem. 277*, 38339–38344.
5. Mees, A., Klar, T., Gnau, P., Hennecke, U., Eker, A. P. M., Carell, T., and Essen, L.-O. (2004) Crystal Structure of a Photolyase Bound to a CPD-Like DNA Lesion After in Situ Repair. *Science 306*, 1789–1793.
6. Maul, M. J., Barends, T. R. M., Glas, A. F., Cryle, M. J., Domratcheva, T., Schneider, S., Schlichting, I., and Carell, T. (2008) Crystal Structure and Mechanism of a DNA (6−4) Photolyase. *Angew. Chem., Int. Ed. 47*, 10076–10086.
7. Malhotra, K., Kim, S.-T., Batschauer, A., Dawut, L., and Sancar, A. (1995) Putative Blue-Light Photoreceptors from *Arabidopsis thaliana* and *Sinapis alba* with a High Degree of Sequence Homology to DNA Photolyase Contain the Two Photolyase Cofactors but Lack DNA Repair Activity. *Biochemistry 34*, 6892–6899.
8. Selby, C. P., and Sancar, A. (2006) A cryptochrome/photolyase class of enzymes with single-stranded DNA-specific photolyase activity. *Proc. Natl. Acad. Sci. U.S.A. 103*, 17696–17700.
9. Stanewsky, R., Kaneko, M., Emery, P., Beretta, B., Wagner-Smith, K., Kay, S. A., Robash, M., and Hall, J. C. (1998) The cry^b Mutation Identifies Cryptochrome as a Circadian Photoreceptor in *Drosophila*. *Cell 95*, 669–679.
10. Cashmore, A. R. (2003) Cryptochromes: Enabling Plants and Animals to Determine Circadian Time. *Cell 114*, 537–543.
11. Yuan, Q., Metterville, D., Briscoe, A. D., and Reppert, S. M. (2007) Insect Cryptochromes: Gene Duplication and Loss Define Diverse Ways to Construct Insect Circadian Clocks. *Mol. Biol. Evol. 24*, 948–955.
12. Sancar, A. (2004) Regulation of the Mammalian Circadian Clock by Cryptochrome. *J. Biol. Chem. 279*, 34079–34082.
13. Gegear, R. J., Casselman, A., Waddell, S., and Reppert, S. M. (2008) Cryptochrome mediates light-dependent magnetosensitivity in *Drosophila*. *Nature 454*, 1014–1018.
14. Brudler, R., Hitomi, K., Daiyasu, H., Toh, H., Kucho, K., Ishiura, M., Kanehisa, M., Roberts, V. A., Todo, T., Tainer, J. A., and Getzoff, E. D. (2003) Identification of a New Cryptochrome Class: Structure, Function, and Evolution. *Mol. Cell 11*, 59–67.
15. Hitomi, K., Okamoto, K., Daiyasu, H., Miyashita, H., Iwai, S., Toh, H., Ishiura, M., and Todo, T. (2000) Bacterial cryptochrome and photolyase: Characterization of two photolyase-like genes of *Synechocystis* sp. PCC6803. *Nucleic Acids Res. 28*, 2353–2362.
16. Worthington, E. N., Kavakli, Ì. H., Berrocal-Tito, G., Bondo, B. E., and Sancar, A. (2003) Purification and Characterization of Three Members of the Photolyase/Cryptochrome Family Blue-light Photoreceptors from *Vibrio cholerae*. *J. Biol. Chem. 278*, 39143–39154.
17. Zikihara, K., Ishikawa, T., Todo, T., and Tokutomi, S. (2008) Involvement of Electron Transfer in the Photoreaction of Zebrafish Cryptochrome-DASH. *Photochem. Photobiol. 84*, 1016–1023.
18. Daiyasu, H., Ishikawa, T., Kuma, K.-i., Iwai, S., Todo, T., and Toh, H. (2004) Identification of cryptochrome-DASH from vertebrates. *Genes Cells 9*, 479–495.
19. Klar, T., Pokorny, R., Moldt, J., Batschauer, A., and Essen, L.-O. (2007) Cryptochrome 3 from *Arabidopsis thaliana*: Structural and Functional Analysis of its Complex with a Folate Light Antenna. *J. Mol. Biol. 366*, 954–964.
20. Huang, Y., Baxter, R., Smith, B. S., Partch, C. L., Colbert, C. L., and Deisenhofer, J. (2006) Crystal structure of cryptochrome 3 from

Arabidopsis thaliana and its implications for photolyase activity. *Proc. Natl. Acad. Sci. U.S.A. 103*, 17701–17706.
21. Pokorny, R., Klar, T., Hennecke, U., Carell, T., Batschauer, T., and Essen, L.-O. (2008) Recognition and repair of UV lesions in loop structures of duplex DNA by DASH-type cryptochrome. *Proc. Natl. Acad. Sci. U.S.A. 105*, 21023–21027.
22. Jorns, M. S., Sancar, G. B., and Sancar, A. (1984) Identification of a Neutral Flavin Radical and Characterization of a Second Chromophore in *Escherichia coli* DNA Photolyase. *Biochemistry 23*, 2673–2679.
23. Miki, K., Tamada, T., Nishida, H., Inaka, K., Yasui, Q., de Ruiter, P. E., and Eker, A. P. M. (1993) Crystallization and Preliminary X-ray Diffraction Studies of Photolyase (Photoreactivating Enzyme) from the Cyanobacterium *Anacystis nidulans*. *J. Mol. Biol. 233*, 167–169.
24. Hitomi, K., DiTacchio, L., Arvai, S., Yamomoto, J., Kim, S.-T., Todo, T., Tainer, J. A., Iwai, S., Panda, S., and Getzoff, E. D. (2009) Functional motifs in the (6−4) photolyase crystal structure make a comparative framework for DNA repair photolyases and clock cryptochromes. *Proc. Natl. Acad. Sci. U.S.A. 106*, 6962–6967.
25. Payne, G., Heelis, P. F., Rohrs, B. R., and Sancar, A. (1987) The Active Form of *Escherichia* DNA Photolyase Contains a Fully Reduced Flavin and Not a Flavin Radical, both in Vivo and in Vitro. *Biochemistry 26*, 7121–7127.
26. Mayhew, S. G. (1999) The effects of pH and semiquinone formation on the oxidation-reduction potentials of flavin mononucleotide. *Eur. J. Biochem. 265*, 698–702.
27. Gindt, Y. M., Schelvis, J. P. M., Thoren, K. L., and Huang, T. H. (2005) Substrate Binding Modulates the Reduction Potential of DNA Photolyase. *J. Am. Chem. Soc. 127*, 10472–10473.
28. Balland, V., Byrdin, M., Eker, A. P. M., Ahmad, M., and Brettel, K. (2009) What Makes the Difference between a Cryptochrome and DNA Photolyase? A Spectroelectrochemical Comparison of the Flavin Redox Transitions. *J. Am. Chem. Soc. 131*, 426–427.
29. Malholtra, K., Kim, S.-T., Walsh, C., and Sancar, A. (1992) Roles of FAD and 8-Hydroxy-5-deazaflavin Chromophores in Photoreactivation by *Anacystis nidulans* DNA Photolyase. *J. Biol. Chem. 267*, 15406–15411.
30. Jorns, M. S., Baldwin, E. T., Sancar, G. B., and Sancar, A. (1987) Action Mechanism of *Escherichia coli* DNA Photolyase. *J. Biol. Chem. 262*, 486–491.
31. Henbest, K. B., Maeda, K., Hore, P. J., Joshi, M., Bacher, A., Bittl, R., Weber, S., Timmel, C. R., and Schleicher, E. (2008) Magnetic-field effect on the photoactivation reaction of *Escherichia coli* DNA photolyase. *Proc. Natl. Acad. Sci. U.S.A. 105*, 14395–14933.
32. Xu, L., Mu, W., Ding, Y., Luo, Z., Han, Q., Bi, F., Wang, Y., and Song, Q. (2008) Active Site of *Escherichia coli* DNA Pohtolyase: Asn378 Is Crucial both for Stabilizing the Neutral Flavin Radical Cofactor and for DNA Repair. *Biochemistry 47*, 8736–8743.
33. Ludwig, M. L., Pattridge, K. A., Metzger, A. L., and Dixon, M. M. (1997) Control of Oxidation-Reduction Potentials in Flavodoxin from *Clostridium beijerinckii*: The Role of Conformation Changes. *Biochemistry 36*, 1259–1280.
34. O'Farrell, P. A., Walsh, M. A., McCarthy, A. A., Higgins, T. M., Voordouw, G., and Mayhew, S. G. (1998) Modulation of the Redox Potentials of FMN in *Desulfovibrio vulgaris* Flavodoxin: Thermodynamic Properties and Crystal Structures of Glycine-61 Mutants. *Biochemistry 37*, 8405–8416.
35. Astuti, Y., Topoglidis, E., Briscoe, P. B., Fantuzzi, A., Gilardi, G., and Durrant, J. R. (2004) Proton-Coupled Electron Transfer of Flavodoxin Immobilized on Nanostructured Tin Dioxide Electrodes: Thermodynamics versus Kinetics Control of Protein Redox Function. *J. Am. Chem. Soc. 126*, 8001–8009.
36. Munro, A. W., Noble, M. A., Robledo, L., Daff, S. N., and Chapman, S. K. (2001) Determination of the Redox Properties of Human NADPH-Cytochrome P450 Reductase. *Biochemistry 40*, 1956–1963.
37. Garnaud, P. E., Koetsier, M., Ost, T. W. B., and Daff, S. (2004) Redox Properties of the Isolated Flavin Mononucleotide- and Flavin Adenine Dinucleotide-Binding Domains of Neuronal Nitric Oxide Synthase. *Biochemistry 43*, 11035–11044.
38. Anusevicius, Z., Miseviciene, Z., Medina, M., Martinez-Julvez, M., Gomez-Moreno, V., and Cenas, N. (2005) FAD semiquinone stability regulates single-and two-electron reduction of quinones by *Anabaena* PCC7119 ferredoxin: $NADP^+$ reductase and its Glu301Ala mutant. *Arch. Biochem. Biophys. 437*, 144–150.
39. Hanley, S. C., Ost, T. W. B., and Daff, S. (2004) The unusual properties of flavocytochrome P450 BM3 flavodoxin domain. *Biochem. Biophys. Res. Commun. 325*, 1418–1423.
40. Byron, C. M., Stankovich, M. T., Husain, M., and Davidson, V. L. (1989) Unusual Redox Properties of Electron-Transfer Flavoprotein from *Methylophilus methylotrophus*. *Biochemistry 28*, 8582–8587.
41. Talfournier, F., Munro, A. W., Basran, J., Sutcliffe, M. J., Daff, S., Chapman, S. K., and Scrutton, N. S. (2001) αArg-237 in *Methylophilus methylotrophus* (sp. W3A1) Electron-transferring Flavoprotein Affords ∼200-Millivolt Stabilization of the FAD Anionic Semiquinone and a Kinetic Block of Full Reduction to the Dihydroquinone. *J. Biol. Chem. 276*, 20190–20196.
42. Massey, V. (1994) Activation of Molecular Oxygen by Flavins and Flavoproteins. *J. Biol. Chem. 269*, 22459–22462.
43. Mattevi, A. (2006) To be or not to be an oxidase: Challenging the oxygen reactivity of flavoenzymes. *Trends Biochem. Sci. 31*, 276–283.
44. Tamada, T., Kitadokoro, K., Higuchi, Y., Inaka, K., Yasui, A., de Ruiter, P. E., Eker, A. P. M., and Miki, K. (1997) Crystal structure of DNA photolyase from *Anacystis nidulans*. *Nat. Struct. Biol. 4*, 887–891.
45. Miyazawa, Y., Nishioka, H., Yura, K., and Yamoto, T. (2008) Discrimination of Class I Cyclobutane Pyrimidine Dimer Photolyase from Blue Light Photoreceptors by Single Methionine Residue. *Biophys. J. 94*, 2194–2203.
46. Wang, B., and Jorns, M. S. (1989) Reconstitution of *Escherichia coli* DNA Photolyase with Various Folate Derivatives. *Biochemistry 28*, 1148–1152.
47. Jorns, M. S., Wang, B., Jordan, S. P., and Chanderkar, L. P. (1990) Chromophore Function and Interaction in *Escherichia* coli DNA Photolyase: Reconstitution of the Apoenzyme with Pterin and/or Flavin Derivatives. *Biochemistry 29*, 552–561.
48. Li, J., Uchida, T., Ohta, T., Todo, T., and Kitagawa, T. (2006) Characteristic Structure and Environment in FAD Cofactor of (6-4) Photolyase along Function Revealed by Resonance Raman Spectroscopy. *J. Phys. Chem. B 110*, 16724–16732.
49. Massey, V., and Hemmerich, P. (1977) A Photochemical Procedure for Reduction of Oxidation- Reduction Proteins Employing Deazariboflavin as Catalyst. *J. Biol. Chem. 252*, 5612–5614.
50. Nöll, G. (2008) Spectroscopic investigation of flavoproteins: Mechanistic differences between (electro)chemical and photochemical reduction and oxidation. *J. Photochem. Photobiol., A 200*, 34–38.
51. Bouly, J. P., Schleicher, E., Dionisio-Sese, M., Vandenbussche, F., Straeten, D., Bakrim, N., Meier, S., Batschauer, A., Galland, P., Bittl, R., and Ahmad, M. (2007) Cryptochrome Blue Light Photoreceptors Are Activated through Interconversion of Flavin Redox States. *J. Biol. Chem. 282*, 9383–9391.
52. Banerjee, R., Schleicher, E., Meier, S., Viana, R. M., Pokorny, R., Ahmad, M., Bittl, R., and Batschauer, A. (2007) The Signaling State of *Arabidopsis* Cryptochrome 2 Contains Flavin Semiquinone. *J. Biol. Chem. 282*, 14916–14922.
53. Hoang, N., Schleicher, E., Kacprzak, S., Bouly, J.-P., Picot, M., Wu, W., Berndt, A., Wolf, E., Bittl, R., and Ahmad, M. (2008) Human and *Drosophila* Cryptochromes Are Light Activated by Flavin Photoreduction in Living Cells. *PLoS Biol. 6*, 1559–1569.
54. Öztürk, N., Song, S.-H., Selby, C., and Sancar, A. (2008) Animal Type 1 Cryptochromes: Analysis of the Redox State of the FAD Cofactor by Site-Directed Mutagenesis. *J. Biol. Chem. 283*, 3256–3263.
55. Xu, L., Zhang, D., Mu, W., van Berkel, W. J. H., and Luo, Z. (2006) Reversible resolution of flavin and pterin cofactors of His-tagged *Escherichia coli* DNA photolyase. *Biochim. Biophys. Acta 1764*, 1454–1461.
56. Schramm, V. L. (2007) Binding Isotope Effects: Boon and Bane. *Curr. Opin. Chem. Biol. 11*, 529–536.
57. Lostao, A., Gómez-Moreno, C., Mayhew, S. G., and Sancho, J. (1997) Differential Stabilization of the Three FMN Redox Forms by Tyrosine 94 and Tryptophan 57 in Flavodoxin from *Anabena* and Its Influence on the Redox Potential. *Biochemistry 36*, 14334–14344.
58. Payne, G., Wills, M., Walsh, C., and Sancar, A. (1990) Reconstitution of *Escherichia coli* Photolyase with Flavins and Flavin Analogues. *Biochemistry 29*, 5706–5711.
59. Petlicki, J., and van de Ven, T. G. M. (1998) The equilibrium between the oxidation of hydrogen peroxide by oxygen and the dismutation of peroxyl or superoxide radicals in aqueous solutions in contact with oxygen. *J. Chem. Soc., Faraday Trans. 94*, 2763–2767.
60. Schleicher, E., Hitomi, K., Kay, C. W. M., Getzoff, E. D., Todo, T., and Weber, S. (2007) Electron Nuclear Double Resonance Differentiates Complementary Roles for Active Site Histidines in (6-4) Photolyase. *J. Biol. Chem. 282*, 4738–4747.

61. Weber, S., Möbius, G., Richter, G., and Kay, C. W. M. (2001) The Electronic Structure of the Flavin Cofactor in DNA Photolyase. *J. Am. Chem. Soc. 123*, 3790–3798.
62. Li, Y. F., Heelis, P. F., and Sancar, A. (1991) Active Site of DNA Photolyase: Tryptophan-206 Is the Intrinsic Hydrogen Atom Donor Essential for Flavin Radical Photoreduction and DNA Repair *in Vitro*. *Biochemistry 30*, 6322–6329.
63. Hitomi, K., Nakamura, H., Kim, S.-T., Mizukoshi, T., Ishikawa, T., Iwai, S., and Todo, T. (2001) Role of Two Histidines in the (6-4) Photolyase Reaction. *J. Biol. Chem. 276*, 10103–10109.
64. Sancar, G. B., Smith, F. W., and Heelis, P. F. (1987) Purification of the Yeast PHR1 Photolyase from an *Escherichia coli* Overproducing Strain and Characterization of the Intrinsic Chromophores of the Enzyme. *J. Biol. Chem. 262*, 15457–15465.